Journal of Magnetism and Magnetic Materials 556 (2022) 169442

Contents lists available at ScienceDirect

Journal of Magnetism and Magnetic Materials

journal homepage: www.elsevier.com/locate/jmmm

Structural and magnetic properties of FeRh films grown on MgO(0 0 1), MgO(0 1 1) and MgO(1 1 1) substrates

Hardeep Kumar [a,*], Sergio L. Morelhao [b], Gerson Pessotto [c], Hardepinder Singh [a], Anil K. Sinha [d], Daniel R. Cornejo [c,*]

[a] Department of Physics, National Institute of Technology Uttarakhand, Srinagar Garhwal 246174, India
[b] Department of Applied Physics, Institute of Physics, University of São Paulo, São Paulo 05508-090, Brazil
[c] Department of Materials and Mechanics, Institute of Physics, University of São Paulo, São Paulo 05508-090, Brazil
[d] Department of Physics, School of Engineering, University of Petroleum and Energy Studies, Bidholi, Uttarakhand 248007, India

ARTICLE INFO

Keywords:
FeRh alloy
Thin films
Epitaxy
Phase transition
Magnetism

ABSTRACT

FeRh thin films are grown on MgO(0 0 1), MgO(0 1 1) and MgO(1 1 1) single-crystal substrates at 600 °C by dc magnetron sputtering and post-annealed at the same temperature for 1 h. Effect of substrate orientation on structural and magnetic properties of FeRh films is studied using X-ray diffraction (Cu-K_α and synchrotron radiation), temperature, and field dependent magnetization measurements. FeRh(0 0 1), (1 1 2), (0 1 1) orientated films with CsCl ordering are obtained on MgO(0 0 1), MgO(0 1 1) and MgO(1 1 1) substrates, respectively. Epitaxial quality of FeRh(0 0 1) is relatively better than FeRh(1 1 2) and FeRh(0 1 1) films. The FeRh(0 1 1) film grows on two orientation relationships: Nishiyama-Wassermann (NW) and Kurdjumov-Sachs (KS). Temperature-dependent out-plane XRD measurements indicate an increase in c-parameter ~0.56% to 0.62% across the AF-FM phase transition. The c/*a* ratio indicate that FeRh(0 0 1) film has in-plane compressive strain, while FeRh(1 1 2) and FeRh(0 1 1) films have tensile strain. The c/*a* ratio and temperature-dependent magnetization measurements (M–T) indicate that AF-FM phase transition can be tuned by appx. 52 K (388 K to 440 K) by variation of lattice strain at FeRh/MgO interface. Thermal hysteresis of appx. 12.8 K, 17 K and 22.9 K is observed for FeRh(0 0 1), FeRh(1 1 2) and FeRh(0 1 1) thin films. Larger thermal hysteresis is expected due to relatively poor epitaxial quality of the FeRh(1 1 2) and FeRh(0 1 1) films as compared to FeRh(0 0 1) film. The larger remnant FM component is observed in nominal AF state (room temperature) in all the samples, and is expected due to combined effect of composition inhomogeneity, substrate-induced strain and defects.

1. Introduction

The near-equiatomic bulk FeRh alloy shows first-order phase transition from antiferromagnetic (AF) α" phase to ferromagnetic (FM) α' phase upon heating at a transition temperature (T_t) ~350 K [1,2]. Both α'and α" phases are chemically ordered with CsCl structure. The AF-FM phase transition in bulk FeRh is accompanied by an isotropic lattice expansion by ~1% without symmetry change, thermal hysteresis of ~10 K, large change in entropy, change in local magnetic structure and electrical resistivity [2–7]. The T_t can be tuned by sample preparation conditions [8–10], heat treatment [11–13], composition [14–16], doping [17–21], applied magnetic field [19,20] and pressure (strain) [22–27] in bulk & thin films of FeRh. In recent years, FeRh epitaxial films have drawn much attention as compared to its bulk counterpart, because of its potential use in various technological applications such as thermally assisted magnetic recording (TAMR) media [28,29], low-power magneto-electric random access memory (MeRAM) [30–32] and antiferromagnetic memory devices [33,34]. Compressive/tensile strain can be induced in epitaxial films due to lattice mismatch between substrate and film. Most studies on epitaxial FeRh films are focused on (0 0 1) oriented films grown on MgO(0 0 1) substrate [9,10,13,15,16,20,21,24–28,34–44]. Besides (0 0 1) substrates of different lattice parameter such as $SrTiO_3$, $LaAlO_3$, and $KTaO_3$ among others, the properties of FeRh films on substrates of other orientations as Al_2O_3(0001) and MgO(1 1 1) have also been investigated [24–27,30–32]. It is observed that in-plane compressive strain shifts the T_t to higher value (i.e. FM phase is stabilized), while in-plane tensile strain shifts the T_t to lower value (i.e. AF phase is stabilized) [24–27].

* Corresponding authors.
E-mail addresses: hardeepkumar@nituk.ac.in (H. Kumar), cornejo@if.usp.br (D.R. Cornejo).

https://doi.org/10.1016/j.jmmm.2022.169442
Received 8 December 2021; Received in revised form 25 April 2022; Accepted 1 May 2022
Available online 5 May 2022

Bordel et al. reported that FeRh films with compressive/tensile strain exhibit perpendicular/in-plane magnetic anisotropy in FM state. Another important observation is that the Fe spin reorientation takes place across the AF-FM phase transition in strained FeRh films [37]. It is important to mention that the thermal hysteresis in FeRh thin films is relatively broader (≥15 K) than its bulk counterpart [24–27,33,35,36,40–42,44]. Film structure and magnetic properties of body centered cubic (*bcc*) thin films such as Fe, FeCo and Fe_3Si depend upon film orientation and the substrate employed [45–48]. The face centered cubic (*fcc*) MgO(0 0 1), MgO(0 1 1) and MgO(1 1 1) substrates have been commonly employed to investigate the effect of film orientation on structural, magnetic and transport properties of *bcc* thin films [45–47]. Effect of film orientation on structure and AF-FM phase transition characteristics of FeRh films is missing in literature. Aim of present work is to study the effect of film orientation on the structure and AF-FM phase transition characteristics of FeRh films grown on MgO(0 0 1), MgO(0 1 1) and MgO(1 1 1) substrates.

2. Thin film growth and experimental details

The FeRh thin films have been grown on MgO(0 0 1), MgO(0 1 1) and MgO(1 1 1) substrates all together using dc magnetron sputtering from Fe and Rh targets (99.99% purity). Homogeneity among different substrates is ensured by fixing substrates at identical positions on the circumference of a circular substrate holder, and substrate holder was rotated at constant speed of 20 rpm. Base pressure of sputtering chamber was better than 2×10^{-7} torr and substrates were introduced into the chamber through load-lock. The substrates were kept at 600 °C for 3 h prior to deposition in order to get clean substrate surfaces. The targets were pre-sputtered for 10 min before deposition. The FeRh films were grown using high purity Ar gas at 2 mtorr pressure. After the deposition, the films were vacuum annealed at 600 °C for 1 h to promote the CsCl-ordered structure (B2). The annealed FeRh films on MgO(0 0 1), MgO(0 1 1) and MgO(1 1 1) substrates are denoted as S1, S2 and S3, respectively in the present study.

Rutherford backscattering spectroscopy (RBS) was used to determine the film thickness and elemental composition. RBS measurements were carried out using 2.2 MeV He^+ ions using a detector placed at scattering angle of 170° in a pelletron-type accelerator. (LAMFI-USP, Brazil). The RBS data was analyzed using MultiSIMNRA software [49]. The MultiSIMNRA software uses computational algorithms to minimize an objective function running multiple instances of SIMNRA software [50], thus finding the set of parameters that best fits simultaneously all experimental data [49]. The structural investigation was carried out using X-ray diffraction (XRD). The growth direction and out-plane lattice parameter (c-parameter) was estimated using out-plane ω/2θ scans using Bruker diffractometer (Cu-k_α, λ = 1.5418 Å). The mosaic spreading and in-plane epitaxial relationship at FeRh/MgO substrate's interface was determined using rocking curve and Phi (ϕ) scan measurements using Cu-$k\alpha_1$ radiation (λ = 1.54056 Å). The in-plane lattice parameter (*a*-parameter) of FeRh film was estimated using in-plane ω/2θ scans/asymmetric reflections having in-plane component at synchrotron XRD2 beamline (LNLS, Brazil) using incident photons of 8.048 keV energy. Temperature dependent out-plane ω/2θ scans were measured across the AF-FM phase transition during heating & cooling cycles at synchrotron XRD2 beamline, LNLS, Brazil using incident photons of 8.048 keV or at BL-12 beamline, Indus-2, India using incident photons of 15.477 keV. Temperature and field dependent magnetization measurements (M–T and M–H) were carried out using a vibrating sample magnetometer (VSM) to study the AF-FM phase transition characteristics.

3. Results and discussion

3.1. Composition and thickness analysis

Fig. 1 shows the typical experimental RBS spectra along with simulated curve for sample S1. The two-layer MgO/FeRh model assuming the uniform FeRh composition failed to fit the RBS data. In order to describe the realistic description of the composition of FeRh, the FeRh layer was sub-divided into four layers to improve the fitting. The quality of fit was evaluated by reduced χ^2 in the MultiSIMNRA software [49]. The FeRh layer was subdivided into sublayers until the reduced χ^2 does not decrease by significant number during simulation. Simulated four-layer structure of FeRh is MgO(Fe,Rh)/$Fe_{49.3}Rh_{50.7}$/$Fe_{23.2}Rh_{76.8}$/Fe_3O_4. The Fe_3O_4 is the top layer (~5 nm thick) formed at the FeRh/air interface. The $Fe_{23.2\pm15.95}$ $Rh_{76.8\pm15.95}$ is the second layer (5.7 nm), the Rh-rich layer is expected to form due to Fe-deficiency in the layers below the top Fe_3O_4 layer. The third layer is $Fe_{49.3\pm0.58}$ $Rh_{50.7\pm0.58}$ and is 89 nm thick. The MgO(Fe, Rh) is the bottom layer adjacent to MgO substrate; it is expected to form due to interfacial diffusion at MgO/FeRh interface. Diffusion of Fe and Rh elements into MgO substrate is evident by the tail in lower channel numbers of Fe and Rh peaks; diffusion of Fe and Rh is evident from circled region in the inset of Fig. 1. Formation of interfacial diffusion layer is reported for MgO/Fe tunnel-junctions [51,52] and MgO/FeRh system deposited/annealed at temperatures higher than 450 °C [36,53]. In current work, the film deposition and annealing is carried out at 600 °C, so similar effect is expected. For simplicity, the four-layer structured FeRh film is designated as FeRh unless specified in whole work.

3.2. Structural investigation

Fig. 2 shows ω/2θ scans along the surface normal direction of the samples. In all cases, diffraction peaks of the FeRh films stand for the CsCl-type of ordered structure that is the B2 phase of FeRh. The substrate-induced film orientation is evident from the XRD patterns in Fig. 2: FeRh(0 0 1)/MgO(0 0 1), FeRh(1 1 2)/MgO(0 1 1), and FeRh(0 1 1)/MgO(1 1 1). The FeRh peaks are not perfectly symmetric but have tail at lower angles for all the three samples similar to Bull et al. [53]. However, the FeRh peaks could not be fitted by a doublet Voigt function by assigning one of the component peak to bulk (relaxed) FeRh with c_0 of 2.9978 Å used in ref. 53, neither by using c_0 of 2.988 Å for bulk FeRh (in AF state) [1,3]. It is concluded that 100% of FeRh film is strained in all the studied samples. One of the possible reasons of asymmetric FeRh peak with tail may be the coexistence of FM and AF phases at room

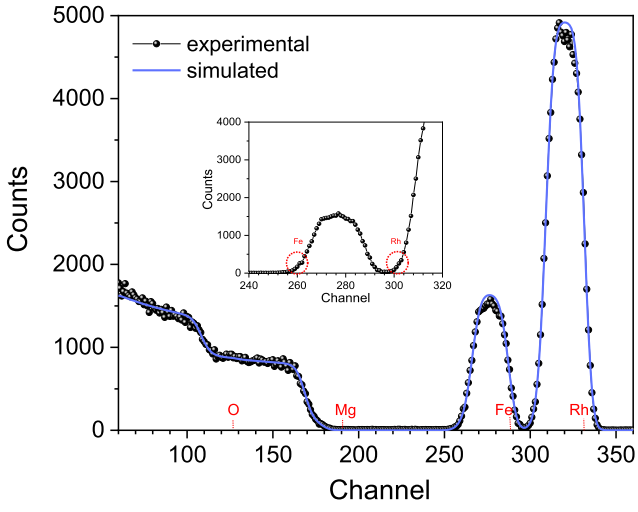

Fig. 1. RBS spectrum along with simulated curve. Diffusion of Fe and Rh elements is evident by circled region in inset of figure.

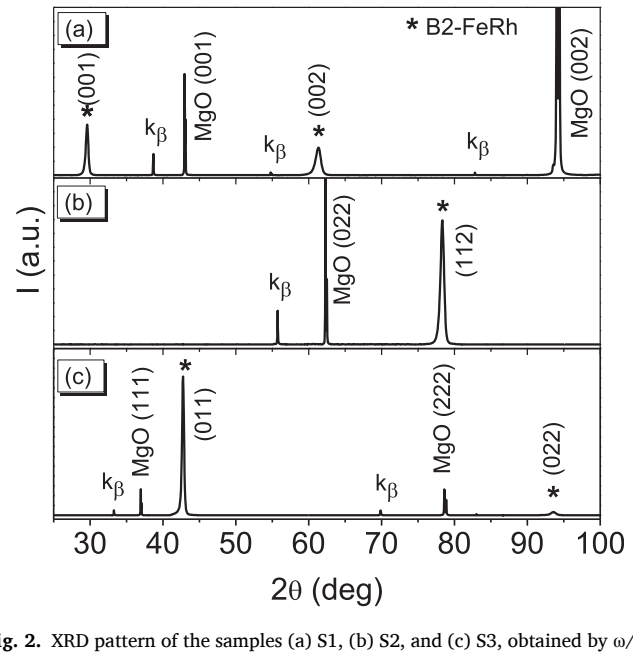

Fig. 2. XRD pattern of the samples (a) S1, (b) S2, and (c) S3, obtained by ω/2θ scans along the film surface normal direction that is different for each sample. Peaks (*) related to the CsCl-type ordering, B2 phase, are seen in all cases.

temperature. Bragg plane d-spacing of 002 (sample S1), 112 (sample S2), and 022 (sample S3) reflections corresponding to AF phase is determined from their peak 2θ positions. For the sake of comparison, the c-parameter calculated from the out-of-plane d-spacing values are reported here as 3.028 Å, 2.986 Å and 2.996 Å for samples S1, S2, and S3, respectively in AF state.

Fig. 3 shows the rocking curves of the 001, 112, and 011 film reflections, corresponding to samples S1, S2, and S3, respectively. Line-profile fitting with pseudo-Voigt functions provide values of 0.86°, 0.94° and 1.97° for the full width at half maximum (FWHM) of FeRh reflections as a measure of mosaicity in the films of samples S1, S2, and S3, respectively. However, to quantitatively compare these mosaicity values it is necessary to convert them into the transversal broadening $\Delta Q_{in\text{-}plane} = Q.\Delta\omega.FWHM$ of the reciprocal lattice points [54], that is perpendicular to the diffraction vector of modulus $Q = 2\pi/d$, as reflections of different d-spacing have been used. The aforementioned FWHM values provide $\Delta Q_{in\text{-}plane} = 0.032$ Å^{-1} (sample S1), 0.084 Å^{-1} (sample S2), and 0.102 Å^{-1} (sample S3). Transversal broadening is caused by reduced domain lateral sizes as well as angular misalignment of the domains. Smaller the $\Delta Q_{in\text{-}plane}$ values, better the crystalline quality of the film in the sense of larger diffracting domains and lower degree of angular misalignment. For example, in the case of negligible angular misalignment, the minimum values of lateral domain sizes that can be inferred are about 20 nm (sample S1), 7.4 nm (sample S2), and 6.2 nm (sample S3). The structural parameters extracted from XRD measurements are summarized in Table 1.

Fig. 4 shows the ϕ-scan curves and epitaxial relationship at FeRh/MgO interface for all the samples. The ϕ-scan of sample S1 is measured by utilizing MgO{4 2 0} and FeRh{2 1 0} asymmetric reflections (see left panel of Fig. 4(a)). Four equidistant peaks separated by 90° are observed for both MgO{4 2 0} and FeRh{2 1 0}, however the FeRh peaks are shifted by 45° relative to MgO peaks. It indicates the four-fold symmetry of both MgO(0 0 1) substrate and FeRh(0 0 1) film, and FeRh[1 0 0] is rotated with respect to MgO[1 0 0] by 45° around film's normal. Interpreted epitaxial relationship for sample S1 is FeRh(001)[1$\bar{1}$0] ‖ MgO(001)[100] and is schematically represented by right panel of Fig. 4(a). Lattice mismatch (f) and out-plane strain (ε_z) are calculated using lattice parameter of bulk FeRh in AF state ($c_0 = 2.988$ Å) and lattice parameter of MgO substrate $a_s = 4.216$ Å. Out-plane strain (ε_z) is calculated using the expression: $\varepsilon_z = \frac{(c-c_0)}{c_0}$ for all samples, here 'c' is the experimental out-plane lattice parameter of FeRh film. Estimated lattice mismatch (f) for sample S1 is -2.13×10^{-3}. It indicates that a-parameter of FeRh film ($\sqrt{2}.c_0 = 4.225$Å) should compress by 0.21% along in-plane [1 0 0] & [0 1 0] and should expand along out-plane [0 0 1] in order to match the a_s. Out-plane strain (ε_z) induced in FeRh film in sample S1 is 1.34×10^{-2}.

Left panel of Fig. 4(b) shows the ϕ-scan of sample S2. The ϕ-scan is performed by utilizing MgO{2 2 2} and FeRh{2 2 2} asymmetric reflections of MgO(0 1 1) substrate and FeRh film, respectively. Two peaks are observed in ϕ-scan of MgO{2 2 2} and FeRh{2 2 2} indicating the two-fold symmetry of both MgO(0 1 1) substrate and FeRh(1 1 2) in the in-plane. Interpreted epitaxial relationship for sample S2 is FeRh(112)[11$\bar{1}$]‖MgO(011)[0$\bar{1}$1], and is schematically represented by right panel of Fig. 4(b). The observed epitaxial relationship is similar to as reported for Fe, Fe_3Si, FeCo films and Fe/Cr superlattice grown on MgO(0 1 1) substrate [45–47,55]. Estimated lattice mismatch (f) along FeRh[$\bar{1}$10] and FeRh[11$\bar{1}$] is −0.21% and 15.2%, respectively. Out-plane strain (ε_z) induced in FeRh film in sample S2 is -6.7×10^{-4}.

Left panel of Fig. 4(c) shows the ϕ-scan of sample S3. The ϕ-scan is performed by utilizing MgO{4 2 0} asymmetric reflection of MgO(1 1 1) substrate and FeRh{2 1 0} and FeRh{2 1 1} asymmetric reflections of FeRh(0 1 1) film. The ϕ-scan of MgO{4 2 0} shows six peaks, indicating the six-fold symmetry of MgO(1 1 1) substrate. The ϕ-scan of FeRh{2 1 0} and FeRh{2 1 1} asymmetric reflection shows six singlet and six doublet peaks, respectively. FeRh(0 1 1) film is expected to have two-fold symmetry rather than six-fold symmetry as evident from ϕ-scan of FeRh{2 1 0} reflection. When the atomic arrangement on MgO(1 1 1) surface is considered, the FeRh(0 1 1) crystals of type-I is expected to consist of three symmetry equivalent variants namely A, B and C. On the other hand, type-II crystals consist of six symmetry equivalent variants whose orientation is rotated about film's normal by 120° and 60°, respectively. Interpreted epitaxial relation is FeRh(011)[100] ‖MgO(111)[$\bar{1}$10] (type-I) employing FeRh{2 1 0} asymmetric reflection,

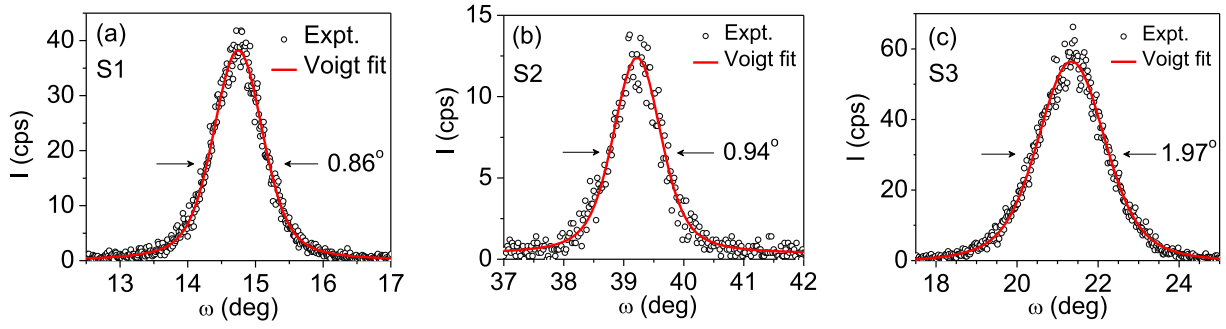

Fig. 3. Rocking curves of film symmetric reflections: (a) 001 (sample S1), (b) 112 (sample S2), and 011 (sample S3). Line-profile fittings with pseudo-Voigt functions (solid red lines) are also shown. (For interpretation of the references to colour in this figure legend, the reader is referred to the web version of this article.)

Table 1
Film orientation, lattice parameter, strain and mosaic spread details of all samples at room temperature.

Sample	Substrate	Film orientation	c (Å) (AF)	Out-plane strain (ϵ_z)	Mosaic spread	a (Å)	c/a ratio
S1	MgO(0 0 1)	(0 0 1)	3.028	1.34×10^{-2}	0.86°	2.971	1.019
S2	MgO(0 1 1)	(1 1 2)	2.986	-6.7×10^{-4}	0.94°	2.993	0.997
S3	MgO(1 1 1)	(0 1 1)	2.996	2.67×10^{-3}	1.97°	3.009	0.996

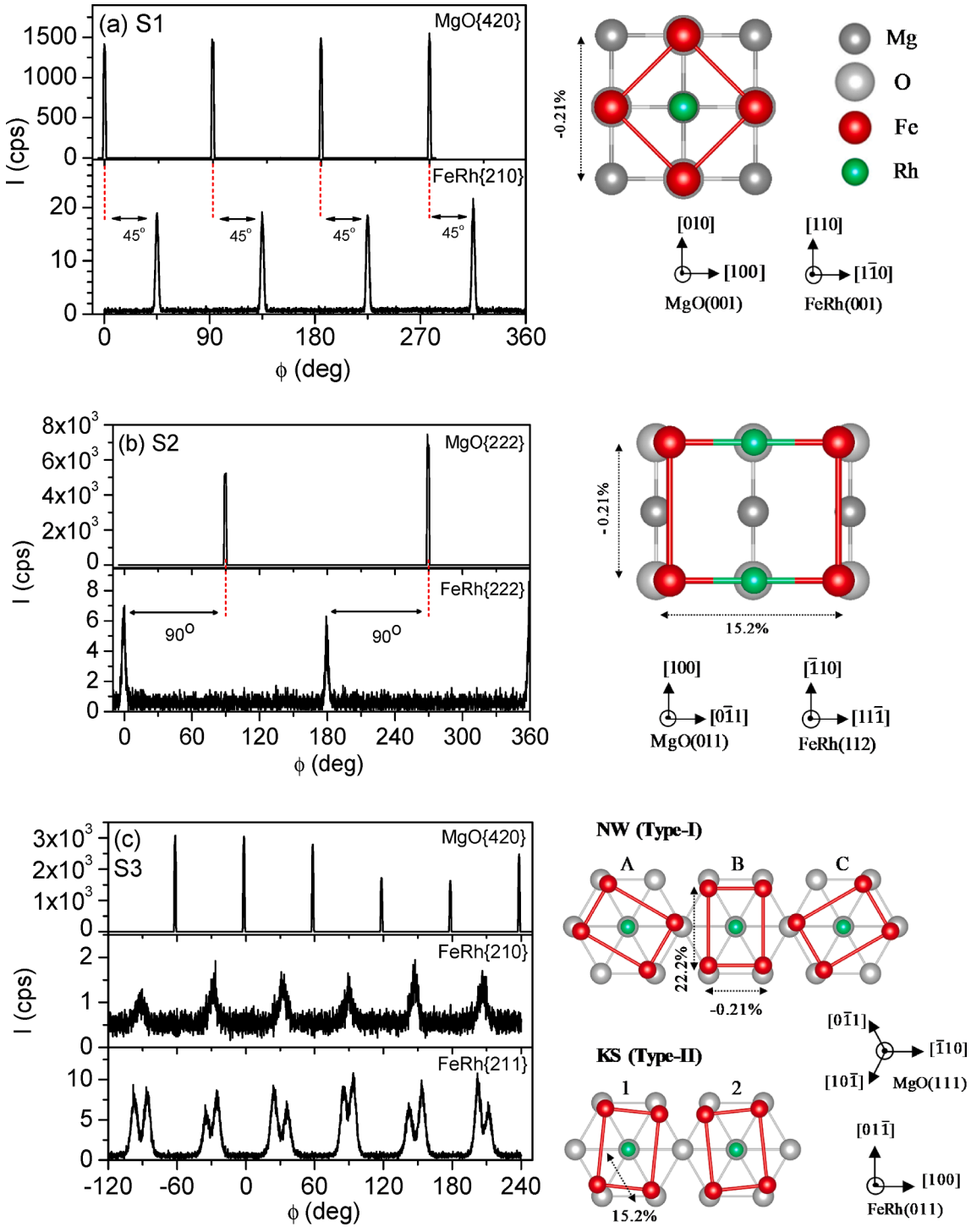

Fig. 4. The ϕ-scan of samples (a) S1, (b) S2 and (c) S3 (left panels). Right panels show the corresponding schematic diagram of epitaxial relationship for all samples. (For interpretation of the references to colour in this figure legend, the reader is referred to the web version of this article.)

while the ϕ-scan of FeRh{2 1 1} asymmetric reflection indicate the epitaxial relation as FeRh(011)[1$\bar{1}$1]||MgO(111)[$\bar{1}$10] (type-II). The epitaxial relationship of type-I and type-II crystals is similar to Nishiyama-Wassermann (NW) [56,57] and Kurdjumov-Sachs (KS) relationship [58], respectively. The KS epitaxial relationship is obtained by $\pm 5.26^{\circ}$ rotation with respect to NW relationship. The ϕ-scan results indicate the co-existence of NW and KS relationship at FeRh(0 1 1)/MgO (1 1 1) interface in sample S3. Three symmetry equivalent variants of NW relationship namely A, B, C are shown in top right panel of Fig. 4(c), two out of six possible symmetry equivalent variants of KS namely 1 and 2 are shown in bottom right panel of Fig. 4(c). Co-existence of NW and KS relationships in sample S3 is in agreement with earlier reports on Fe, and FeCo films grown on MgO(1 1 1) substrate [45–47]. Estimated lattice mismatch along FeRh[1 0 0]$_{NW}$, FeRh[01$\bar{1}$]$_{NW}$ and FeRh[1 $\bar{1}$ 1]$_{KS}$ is −0.21%, 22.2% and 15.2%, respectively. These values indicate that large lattice mismatch is involved in these configurations at FeRh(0 1 1)$_{NW}$/MgO(1 1 1) and FeRh(0 1 1)$_{KS}$/MgO(1 1 1) interface. Out-plane strain (ε_z) induced in FeRh film in sample S3 is 2.67×10^{-3}.

Fig. 5 shows the typical in-plane ω/2θ scans with scattering vector parallel to FeRh [0 1 0] and FeRh[0 $\bar{1}$ 1] for sample S1 and S3, respectively. Estimated *a*-parameter is 2.971 Å, 2.993 Å and 3.009 Å for samples S1, S2 and S3, respectively. Epitaxial strain in FeRh due to substrate is estimated from c/*a* ratio. The c/*a* ratio is 1.019, 0.997 and 0.996 for samples S1, S2 and S3, respectively. The c/*a* value indicate that sample S1 has compressive strain, while samples S2 and S3 has tensile strain. Fig. 6(a-b) shows the typical out-plane ω/2θ scans measured at various temperatures during heating and cooling cycle near FeRh(0 1 1) peak in sample S3 using 8.048 keV photons (λ = 1.54056 Å) at XRD2 beamline, LNLS, Brazil. It is evident that diffraction peak shifts towards lower (higher) angle as temperature increases (decreases) in line with literature [15,41]. However, in few studies single diffraction peak is found to split into two peaks in the AF-FM transition region, indicating the coexistence of AF and FM phase in transition region [40,42–44,59]. Non-observation of doublet peaks is expected due to large temperature steps in the XRD measurements in present case similar to earlier report [15]. Fig. 6(c) shows the variation of extracted *c*-parameter as a function of temperature during heating and cooling cycle. It is evident from Fig. 6(c) that *c*-parameter of FeRh film in sample S3 increases upon heating & decreases upon subsequent cooling to room temperature and exhibit hysteresis behavior and agrees well with literature [15,41,42,44]. Qualitatively similar results are observed for other samples also (not shown). The maximum change in c-parameter across the AF-FM phase transition is estimated to be ~0.62%, 0.56% and 0.56% for samples S1, S2 and S3, respectively.

3.3. Magnetic measurements

Fig. 7(a) shows the temperature dependent magnetization curves (M–T) for all samples measured at magnetic field of 5 kG applied parallel to film plane. It is evident from Fig. 7(a) that magnetization increases with increase in temperature (due to conversion of AF phase to FM phase) and at very high temperature, the magnetization saturates. Estimated saturation magnetization (M_s) is in the range of 900–1000 emu/cm^3 for the studied samples, it is important to mention that observed M_s agrees well with the reported M_s of 700–1300 emu/cm^3. Upon cooling, the magnetization decreases from M_s to a minimum value by conversion of FM phase to AF phase, and exhibit a hysteresis behavior. Transition temperature during heating (T_t) & cooling ($T_t^{'}$) is extracted from the maxima of first-order derivative of magnetization ($\frac{dM}{dT}$) curve. Fig. 7(b) shows the typical temperature dependent variation of $\frac{dM}{dT}$ for sample S1. The estimated T_t and $T_t^{'}$ values are summarized in Table 2. The M–T and XRD measurements (section 3.2) allow us to find the correlation between transition temperature (T_t) and the degree of strain in FeRh lattice in all the samples. It can be interpreted that compressive/tensile strain shifts the T_t to higher/lower value for sample S1/S3. Smaller shift in T_t, $T_t^{'}$ for sample S2 as compared to sample S3 is expected due to relatively smaller tensile strain in sample S2 than S3. The observed trend agrees well with earlier reports [24–27]. Thermal hysteresis (ΔT_t) is estimated from difference of T_t and $T_t^{'}$ values. The ΔT_t value is 12.8 K, 17 K and 22.9 K for samples S1, S2 and S3, respectively. Reported ΔT_t for bulk FeRh and thin films is appx. 10 K and $\geq$ 15 K, respectively [2,3,24–27,33,35,36,40–42,44]. Narrow thermal hysteresis (ΔT_t) in sample S1 is expected due to its better epitaxial quality as compared to samples S2 and S3. Extracted magnetic parameters are summarized in Table 2 for all samples.

Non-zero magnetization in the range of 187–249 emu/cm^3 is observed for the studied samples near room temperature. Non-zero magnetization (in nominal AF state) indicates the presence of a remnant FM phase at near room temperature. The remnant magnetization value is relatively higher than the literature; the observation is supported by the existence of asymmetric FeRh peaks in ω/2θ XRD scans at room temperature. Fig. 8(a-c) show the field-dependent magnetization (M–H) curves measured at high temperature in FM state and near room temperature. A larger coercivity (H_c) is observed at high temperatures as compared to near room temperature. The non-zero but smaller H_c, M_r values around room temperature indicates the coexistence of both FM and AF phases at room temperature, which is well below the transition temperature ($T_t^{'}$). Larger H_c at high temperature indicates the complete conversion of AF phase to FM phase. M–H measurements support the finding of M–T curves around room temperature & observation of FM state at high temperatures. In literature, few recent works

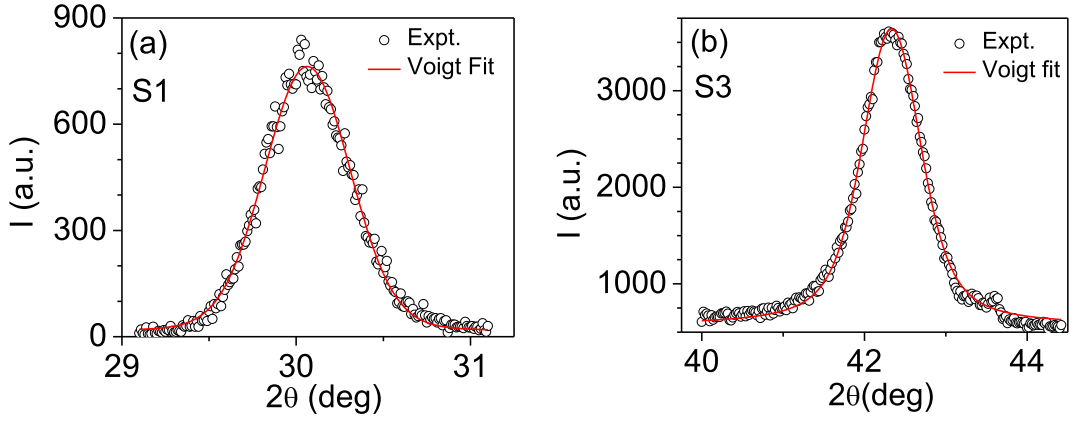

Fig. 5. Typical in-plane ω/2θ scan for samples (a) S1 and (b) S3 measured using Synchrotron radiation. The scattering vector is parallel to FeRh [0 1 0] and FeRh[0 $\bar{1}$ 1] for samples S1 and S3, respectively. (For interpretation of the references to colour in this figure legend, the reader is referred to the web version of this article.)

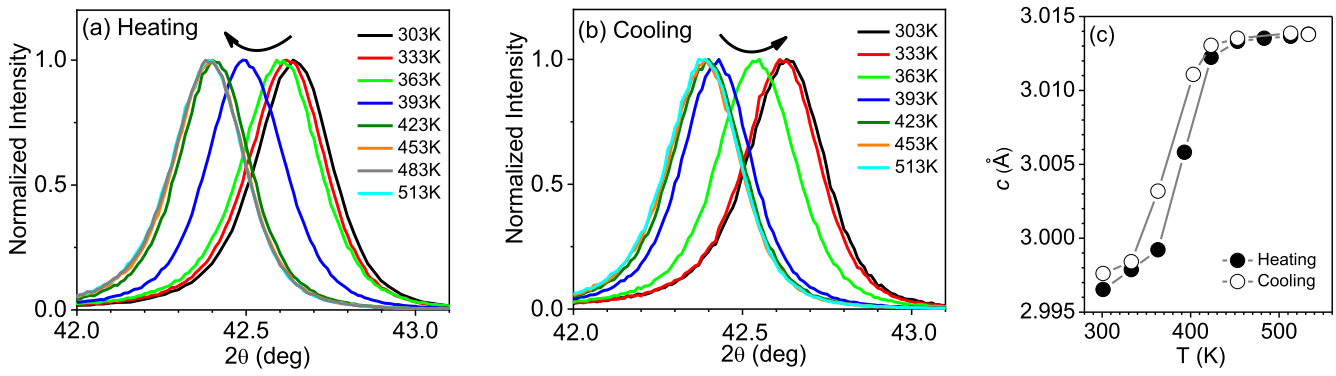

Fig. 6. Out-plane ω/2θ scans measured at various temperatures during (a) heating, (b) cooling cycle near FeRh(0 1 1) peak for sample S3 using synchrotron radiation of λ = 1.54056 Å, (c) extracted temperature dependence of c-parameter during heating & cooling cycle. (For interpretation of the references to colour in this figure legend, the reader is referred to the web version of this article.)

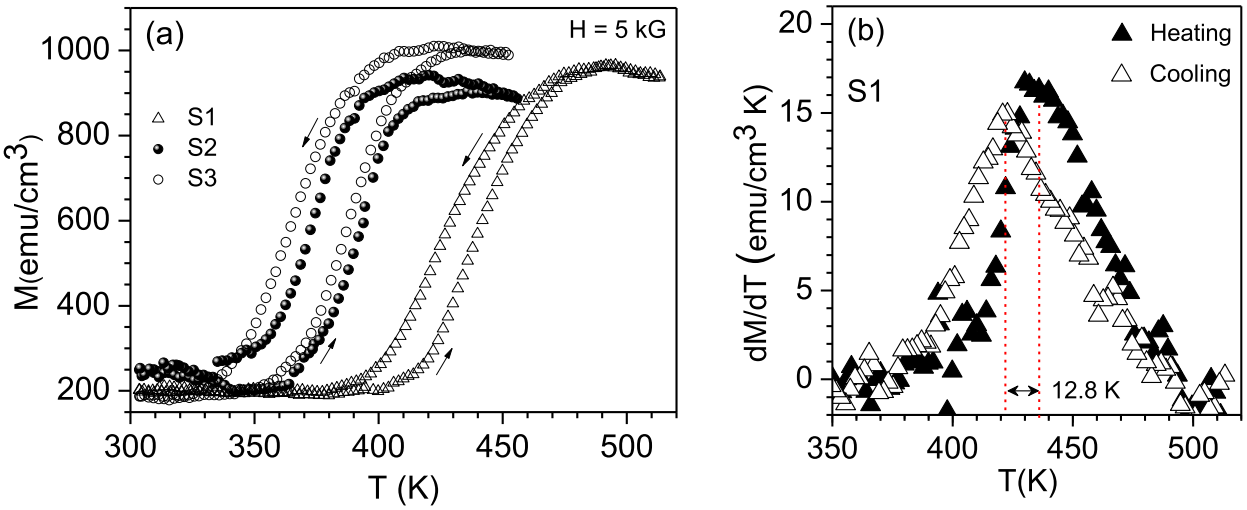

Fig. 7. (a) Temperature dependent magnetization (M–T) curves for samples S1, S2 and S3 with an applied magnetic field of 5 kG parallel to film plane, (b) temperature dependence of $\left|\frac{dM}{dT}\right|$ for sample S1. (For interpretation of the references to colour in this figure legend, the reader is referred to the web version of this article.)

Table 2
Transition temperature (T_t, $T_t^{'}$) , thermal hysteresis (ΔT_t), saturation magnetization (M_s) and retained FM parameters extracted from M–T curves for all samples.

Sample	T_t (K) (Heating)	$T_t^{'}$(K) (Cooling)	ΔT_t (K)	M_s (emu/cm^3)	Retained FM in AF state (emu/cm^3)
S1	440.2	427.4	12.8	965	201
S2	390.6	373.6	17.0	901	249
S3	387.9	365.0	22.9	999	187

report the existence of remnant FM phase in AF state. These studies indicate that remnant FM may be due to composition inhomogeneity, defects or interfacial strain due to substrate [36,38,39,60]. The RBS and XRD analysis indicate the presence of composition inhomogeneity with depth, different density of defects (lateral domain size) and out-plane strain as a function of substrate used. It indicates that observed remnant FM can be due to combination of these effects. However, the exact origin of remnant FM in nominal AF state is not well-understood [26]. Systematic studies on individual effect of composition inhomogeneity, strain and defects will help to understand their role in stabilization of FM phase in AF state.

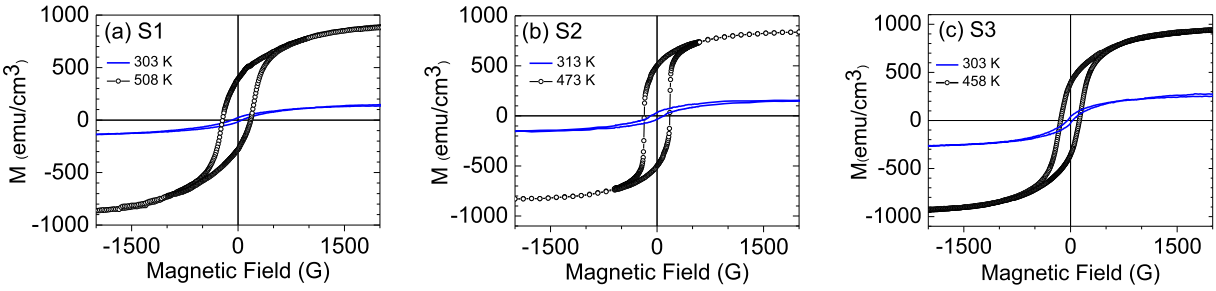

Fig. 8. Field dependent magnetization (M–H) curves measured at a high temperature (in FM state of FeRh) and at near room temperature for samples (a) S1, (b) S2 and (c) S3. (For interpretation of the references to colour in this figure legend, the reader is referred to the web version of this article.)

4. Conclusions

In summary, the FeRh films with (0 0 1), (1 1 2), (0 1 1) preferred orientation are formed on MgO(0 0 1), MgO(0 1 1) and MgO(1 1 1) substrates, respectively. The FeRh(0 0 1) film is single-crystalline in nature. The FeRh(0 1 1) film grows with two epitaxial relationships: Nishiyama-Wassermann (NW) and Kurdjumov-Sachs (KS). The estimated c/*a* values indicate in-plane compressive strain in FeRh film for sample S1, and tensile strain in sample S2 and S3. XRD and magnetic measurements indicate that that AF-FM phase transition in FeRh films can be tuned by appx. 52 K (388 K to 440 K) by the variation of lattice strain at FeRh/MgO interface by the selection of MgO substrate of different orientation. Thermal hysteresis of appx. 12.8 K, 17 K and 22.9 K is observed for FeRh(0 0 1), FeRh(1 1 2) and FeRh(0 1 1) films, respectively. The non-zero remnant magnetization around room temperature indicates the presence of remnant FM phase in addition to major AF phase at near room temperature.

CRediT authorship contribution statement

Hardeep Kumar: Conceptualization, Data curation, Formal analysis, Writing – original draft, Funding acquisition. **Sergio L. Morelhao:** Formal analysis, Writing – review & editing. **Gerson Pessotto:** Investigation, Formal analysis. **Hardepinder Singh:** Investigation, Formal analysis. **Anil K. Sinha:** Investigation, Formal analysis. **Daniel R. Cornejo:** Conceptualization, Writing – review & editing, Supervision, Funding acquisition.

Declaration of Competing Interest

The authors declare that they have no known competing financial interests or personal relationships that could have appeared to influence the work reported in this paper.

Acknowledgements

The work was partially supported by FAPESP, Brazil (process no. 2010/18590-0) and UGC-DAE CSR, Indore, India (ref. no. CSR-IC-ISUM-01/CRS-284/2019-20/1336). Technical support from Sergio Romero, Antonio Carlos Franco da Silveira, Tarsis Mendes Germano, Tiago Fiorini da Silva (IFUSP, Brazil), M. N. Singh (BL-12, Indus 2, India) and Dr. Leide P. Cavalcanti (XRD2, LNLS, Brazil) during characterization works is highly acknowledged. Dr. Cleber L. Rodrigues (LAMFI-USP, Brazil) is specially acknowledged for his help in RBS analysis. H.S. acknowledges MHRD, India for JRF.

References

[1] M. Fallot, Ann. Phys. 11 (10) (1938) 291, https://doi.org/10.1051/anphys/193811100291.
[2] J.S. Kouvel, C.C. Hartelius, J. Appl. Phys. 33 (1962) 1343, https://doi.org/10.1063/1.1728721.
[3] A.I. Zakharov, A. Kadomtseva, R. Levitin, E. Ponyatovskii, J. Expt. Theor. Phys. (USSR) 46 (1964) 1348, http://www.jetp.ras.ru/cgi-bin/e/index/e/19/6/p1348?a=list.
[4] C.J. Schinkel, R. Hartog, F.H.A.M. Hochstenbach, J. Phys. F 4 (1974) 1412, https://doi.org/10.1088/0305-4608/4/9/013.
[5] M.P. Annaorazov, S.A. Nikitin, A.L. Tyurin, K.A. Asatryan, A. Kh Dovletov, J. Appl. Phys. 79 (1996) 1689, https://doi.org/10.1063/1.360955.
[6] L. Zsoldos, Phys. Status Solidi B 20 (1967) K25, https://doi.org/10.1002/pssb.19670200148.
[7] V.L. Moruzzi, P.M. Marcus, Phy. Rev. B 46 (1992) 2864, https://doi.org/10.1103/PhysRevB.46.2864.
[8] J.M. Lommel, J. Appl. Phys. 37 (1966) 1483, https://doi.org/10.1063/1.1708527.
[9] W. Lu, P. Huang, K. Li, B. Yan, J. Mater. Res. 28 (2013) 1042, https://doi.org/10.1557/jmr.2013.61.
[10] V.G. Myagkov, A.A. Ivanenko, L.E. Bykova, V.S. Zhigalov, M.N. Volochaev, D. A. Velikanov, A.A. Matsynin, G.N. Bondarenko, Sci. Rep. 10 (2020) 10807, https://doi.org/10.1038/s41598-020-67837-2.
[11] J.M. Lommel, J.S. Kouvel, J. Appl. Phys. 38 (1967) 1263, https://doi.org/10.1063/1.1709570.
[12] Y. Ohtani, I. Hatakeyama, J. Appl. Phys. 74 (1993) 3328, https://doi.org/10.1063/1.354557.
[13] J. Cao, N.T. Nam, S. Inoue, H.Y.Y. Ko, N.N. Phuoc, T. Suzuki, J. Appl. Phys. 103 (2008) 07F501, https://doi.org/10.1063/1.2828812.
[14] S. Yamada, K. Tanikawa, J. Hirayama, T. Kanashima, T. Taniyama, K. Hamaya, Phys. Rev. B 92 (2015), 094416, https://doi.org/10.1103/PhysRevB.92.094416.
[15] K.M. Cher, T. Zhou, J.S. Chen, IEEE Trans. Magn. 47 (2011) 4033, https://doi.org/10.1109/TMAG.2011.2140363.
[16] A.B. Mei, Y. Tang, J.L. Grab, J. Schubert, D.C. Ralph, D.G. Schlom, Appl. Phy. Lett. 113 (2018), 082403, https://doi.org/10.1063/1.5048303.
[17] P.H.L. Walter, J. Appl. Phys. 35 (1964) 938, https://doi.org/10.1063/1.1713547.
[18] N.V. Baranov, E.A. Barabanova, J. Alloys Compounds 219 (1995) 139, https://doi.org/10.1016/0925-8388(94)01375-6.
[19] P. Kushwaha, A. Lakhani, R. Rawat, P. Chaddah, Phy. Rev. B 80 (2009), 174413, https://doi.org/10.1103/PhysRevB.80.174413.
[20] W. Lu, N.T. Nam, T. Suzuki, J. Appl. Phy. 105 (2009) 07A904, https://doi.org/10.1063/1.3065973.
[21] J. Jia-hui Chen, Y.-J. Ma, L. Wu, C.W. Nan, J. Alloys Compd. 741 (2018) 557, https://doi.org/10.1016/j.jallcom.2018.01.186.
[22] R.C. Wayne, Phy. Rev. 170 (1968) 523, https://doi.org/10.1103/PhysRev.170.523.
[23] L.I. Vinokurova, A.V. Vlasov, M. Pardavi-Horváth, Phy. Status Solidi B 78 (1976) 353, https://doi.org/10.1002/pssb.2220780136.
[24] S. Maat, J.-U. Thiele, and Eric E. Fullerton, Phy. Rev. B 72, 214432 (2005), https://doi.org/10.1103/PhysRevB.72.214432.
[25] A. Ceballos, Zhanghui Chen, O. Schneider, C. Bordel, Lin-Wang Wang and F. Hellman, Appl. Phy. Lett. 111, 172401 (2017), https://doi.org/10.1063/1.4997901.
[26] M.G. Loving, R. Barua, C. Le Graët, C.J. Kinane, D. Heiman, S. Langridge, C. H. Marrows, L.H. Lewis, J. Phys. D: Appl. Phys. 51 (2018), 024003, https://doi.org/10.1088/1361-6463/aa9d1f.
[27] H. Kumar, D.R. Cornejo, S.L. Morelhao, S. Kycia, I.M. Montellano, N.R. Álvarez, G. Alejandro, A. Butera, J. Appl. Phys. 124 (2018), 085306, https://doi.org/10.1063/1.5020160.
[28] J.U. Thiele, S. Maat, E.E. Fullerton, Appl. Phys. Lett. 82 (2003) 2859, https://doi.org/10.1063/1.1571232.
[29] E. Fullerton, S. Maat, and J. U. Thiele, U.S. patent 20050281081 (2005).
[30] R.O. Cherifi et al., Nat. Mater. 13, 345 (2014), https://doi.org/10.1038/nmat3870.
[31] Z. Feng, H. Yan, Z. Liu, Adv. Elect. Mater. 5 (2019) 1800466, https://doi.org/10.1002/aelm.201800466.
[32] H. Yan, Z. Feng, P. Qin, X. Zhou, H. Guo, X. Wang, H. Chen, X. Zhang, H. Wu, C. Jiang, Z. Liu, Adv. Mater. 32 (2020) 1905603, https://doi.org/10.1002/adma.201905603.
[33] I. Fina, N. Dix, E. Menéndez, A. Crespi, M. Foerster, L. Aballe, F. Sánchez, J. Fontcuberta, ACS Appl. Mater. Interfaces 12 (2020) 15389, https://doi.org/10.1021/acsami.0c00704.
[34] X. Marti, et al., Nat. Mater. 13 (2014) 367, https://doi.org/10.1038/nmat3861.
[35] G.C. Han, J.J. Qiu, Q.J. Yap, P. Luo, T. Kanbe, T. Shige, D.E. Laughlin, J.-G. Zhu, J. Appl. Phys 113 (2013), 123909, https://doi.org/10.1063/1.4798275.
[36] C. Baldasseroni, et al., J. Appl. Phys. 115 (2014), 043919, https://doi.org/10.1063/1.4862961.
[37] C. Bordel, J. Juraszek, David W. Cooke, C. Baldasseroni, S. Mankovsky, J. Minár, H. Ebert, S. Moyerman, E.E. Fullerton, F. Hellman, Phy. Rev. Lett. 109, 117201 (2012), https://doi.org/10.1103/PhysRevLett.109.117201.
[38] Y. Ding, D.A. Arena, J. Dvorak, M. Ali, C.J. Kinane, C.H. Marrows, B.J. Hickey, L. H. Lewis, J. Appl. Phys. 103 (2008) 07B515, https://doi.org/10.1063/1.2837247.
[39] R. Fan, et al., Phys. Rev. B 82 (2010), 184418, https://doi.org/10.1103/PhysRevB.82.184418.
[40] J.W. Kim, P.J. Ryan, Y. Ding, L.H. Lewis, M. Ali, C.J. Kinane, B.J. Hickey, C. H. Marrows, D.A. Arena, Appl. Phy. Lett. 95 (2009), 222515, https://doi.org/10.1063/1.3265921.
[41] S. Inoue, H.Y.Y. Ko, T. Suzuki, IEEE Trans. Magn. 44 (2008) 2875, https://doi.org/10.1109/TMAG.2008.2001846.
[42] M.A. de Vries, M. Loving, M. McLaren, R.M.D. Brydson, X. Liu, S. Langridge, L. H. Lewis, C.H. Marrows, Appl. Phy. Lett. 104 (2014), 232407, https://doi.org/10.1063/1.4883369.
[43] D.J. Keavney, Y. Choi, M.V. Holt, V. Uhlíř, D. Arena, E.E. Fullerton, P.J. Ryan, J. W. Kim, Sci. Rep. 8 (2018) 1778, https://doi.org/10.1038/s41598-018-20101-0.
[44] J.A. Arregi, O. Caha, V. Uhlíř, Phy. Rev B 101 (2020), 174413, https://doi.org/10.1103/PhysRevB.101.174413.
[45] B.L. Guo, P. Li, C. Jin, H. Liu, H.L. Bai, Phys. Status Solidi B 251 (2014) 761, https://doi.org/10.1002/pssb.201349193.
[46] K. Serizawa, M. Ohtake, T. Kawai, M. Futamoto, F. Kirino, N. Inaba, J. Magn. Magn. Mater. 477 (2019) 420, https://doi.org/10.1016/j.jmmm.2018.12.020.
[47] K. Shikada, M. Ohtake, F. Kirino, M. Futamoto, J. Appl. Phys. 105 (2009) 07C303, https://doi.org/10.1063/1.3067854.
[48] T. Nishiyama, M. Ohtake, F. Kirino, M. Futamoto, J. Appl. Phys. 107 (2010) 09A306, https://doi.org/10.1063/1.3334200.
[49] T.F. Silva, C.L. Rodrigues, M. Mayer, M.V. Moro, G.F. Trindade, F.R. Aguirre, N. Added, M.A. Rizzutto, M.H. Tabacniks, Nucl. Instrum. Methods Phys. Res. B 371, 86 (2016), https://doi.org/10.1016/j.nimb.2015.10.038.
[50] M. Mayer, AIP Conf. Proc. 475 (1999) 541, https://doi.org/10.1063/1.59188.
[51] S.R. Spurgeon, J.D. Sloppy, R. Tao, R.F. Klie, S.E. Lofland, J.K. Baldwin, A. Misra, M.L. Taheri, J. Appl. Phys. 112 (2012), 013905, https://doi.org/10.1063/1.4730630.

[52] C. Martinez-Boubeta, L. Balcells, B. Martinez, J. Appl. Phys. 113 (2013), 123908, https://doi.org/10.1063/1.4798242.
[53] C. Bull, C.W. Barton, W. Griggs, Caruana, C.J. Kinane, P.W. Nutter, T. Thomson, APL Mater. 7, 101117 (2019), https://doi.org/10.1063/1.5120622.
[54] S.L. Morelhão, S.W. Kycia, S. Netzke, C.I. Fornari, P.H.O. Rappl, E. Abramof, J. Phys. Chem. C 123 (2019) 24818, https://doi.org/10.1021/acs.jpcc.9b05377.
[55] E.E. Fullerton, M.J. Conover, J.E. Mattson, C.H. Sowers, S.D. Bader, Phy. Rev. B 48 (1993) 15755, https://doi.org/10.1103/PhysRevB.48.15755.
[56] G. Wasserman, Arch. Eisenhuettenwes 16 (1933) 647.
[57] Z. Nishiyama, Sci. Rep. Tohoku Univ. 23 (1934) 638, https://cir.nii.ac.jp/crid/1573668925572199168.
[58] G. Kurdjumov, G. Sachs, Z. Phys. 64 (1930) 325, https://doi.org/10.1007/BF01397346.
[59] K. Ohtake, Y. Mitsui, K. Takahashi, R. Onodera, S. Kimura, K. Watanabe, K. Koyama, IEEE Trans. Magn. 50 (2014) 1001404, https://doi.org/10.1109/TMAG.2013.2273363.
[60] C.W. Barton, T.A. Ostler, D. Huskisson, C.J. Kinane, S.J. Haigh, G. Hrkac, T. Thomson, Sci Rep. 7 (2017) 44397, https://doi.org/10.1038/srep44397.